





Cite this: DOI: 10.1039/c7gc00346c

Cellulose and lignin colocalization at the plant cell wall surface limits microbial hydrolysis of *Populus* biomass†

Alexandru Dumitrache,^{a,b} Allison Tolbert,^{a,b,c} Jace Natzke,^{a,b} Steven D. Brown,^{a,b} Brian H. Davison ^{a,b} and Arthur J. Ragauskas ^{*a,b,d}

Biorefining of plant feedstocks into fuels and specialty chemicals, using biological conversion, requires the solubilization of lignocellulosics into simpler oligomeric compounds. However, non-pretreated woody biomass has shown high resistance to hydrolysis by cellulolytic microbes or purified cellulases. We investigate the limited solubilization of *Populus deltoides* by the cellulolytic thermophile *Clostridium thermocellum* in the absence of solute inhibitors. Compared to control samples, fermented poplar revealed that the hydrolysis of carbohydrates in secondary cell walls ceased prematurely as the presence of lignin increased at the surface. In quantitative fluorescence colocalization analysis by confocal laser scanning microscopy, the Manders' coefficient of the fractional overlap between lignin and cellulose signals increased from an average of 0.67 to a near-maximum of 0.92 in fermented tissue. Chemical imaging by time-of-flight secondary ion mass spectrometry revealed a 49% decline in surface cellulose and a compensatory 30% and 11% increase in surface S- and G-lignin, respectively. Although 72% of the initial glucan was still present in the lignocellulose matrix of this feedstock, subsequent treatments with cell-free purified cellulases did not significantly restore hydrolysis. This confirmed that biomass surfaces had become non-productive for the *C. thermocellum* hydrolytic exoproteome. This study provides direct evidence for an explicit definition of feedstock recalcitrance, whereby depletion of surface carbohydrate increases lignin exposure which leads to inhibition of enzyme activity, while the bulk residual biomass retains significant undigested carbohydrate content. The analysis presented here establishes a novel method for the quantitation of lignocellulose recalcitrance.

Received 30th January 2017,
Accepted 10th April 2017

DOI: 10.1039/c7gc00346c

rsc.li/greenchem

Introduction

The native North American species of poplar, including *Populus deltoides*, are fast growing temperate trees and promising lignocellulosic feedstock for a renewable bio-based economy of fuels and value-added chemicals (e.g., 1,4-butanediol, succinate, isoprene).^{1,2} This short-rotation woody crop has growth potential in a variety of ecosystems such as the Great Lake States, the Northwest, and the Mississippi Delta

with a reported 2554 acres of production land in November 2014.³

Biorefinery valorization of lignocellulosic feedstock necessitates the deconstruction of plant cell wall biopolymers into simpler soluble components *via* the biological conversion platform. However, plant tissue presents an intrinsic resistance to deconstruction by purified enzymatic mixtures⁴ or by specialized cellulolytic microbes,⁵ which is largely due to the complex structure of the plant cell wall polymers, specifically cellulose and other heteropolysaccharides along with polyphenolic lignin.⁶ While lignin has potential to add value to a biorefinery, at present it complicates biochemical processes for lignocellulosic biofuels.⁷

Undomesticated natural variants of *Populus deltoides* contain 16–28% w/w lignin, which has been negatively correlated to the extraction of sugars from non-pretreated biomass.⁸ Conversely, increased cellulose exposure to hydrolytic agents has consistently been associated with improved solubilization. For example, mechanically cutting the biomass in a particular way, like tangential to the annual ring, can disrupt cellulose

^aBioenergy Science Center (BESC), Oak Ridge National Laboratory, Oak Ridge, Tennessee, USA

^bBiosciences Division, Energy and Environment Directorate, Oak Ridge National Laboratory, Oak Ridge, Tennessee, USA

^cSchool of Chemistry and Biochemistry & Renewable Bioproducts Institute, Georgia Institute of Technology, Atlanta, Georgia, USA

^dDepartment of Chemical and Biomolecular Engineering, Center for Renewable Carbon, Department of Forestry, Wildlife, and Fisheries, University of Tennessee, Knoxville, Tennessee, USA. E-mail: aragausk@utk.edu

† Electronic supplementary information (ESI) available. See DOI: 10.1039/c7gc00346c

crystallinity and increase the accessible surface area, leading to improved enzymatic hydrolysis.⁹

Clostridium thermocellum is a fast growing, anaerobic and thermophilic cellulolytic bacterium capable of growth on the recalcitrant lignocellulosic material.¹⁰ This well characterized biomass-hydrolyzing organism secretes a wide range of cell-bound and free glycoside hydrolases with an estimated 70 types of cellulosomal and 27 non-cellulosomal enzymes.^{11,12} Extracellular hydrolysis of biomass polysaccharides yields oligomeric hexose and pentose sugars, with the former utilized for energy and growth in anaerobic fermentation. The bacterium is known for efficient hydrolysis of crystalline cellulose to near-completion,^{13,14} and is capable of solubilizing 90% of xylan in dilute acid pretreated corn-stover.¹² Although it is a robust cellulolytic microbe that commonly exceeds the performance of commercial fungal cellulase mixtures, it struggles to depolymerize the complex lignocellulose in the plant cell wall of typical energy grasses¹⁵ and hard woods¹⁶ without significant pretreatment of the feedstock.¹⁷ While recent investigations have focused on the contributions lignin has towards inhibiting fungal cellulases,¹⁸ interaction between lignin and *C. thermocellum* has not been equally defined and needs further investigation, especially in regard to the surface lignin.

To realize the potential of feedstock bioconversion without costly or complex pre-treatments and to understand the major bottlenecks in lignocellulose solubilization, we investigated the cessation of microbial hydrolysis of juvenile poplar tissue by *C. thermocellum* and by cell-free microbial cellulase extracts, in the absence of known soluble inhibitors. We hypothesized that changes in the colocalization and the relative proportion of lignin and cellulose at the surface of plant tissue lead to the premature cessation of hydrolytic activity. To test this, we compared 60 μm thick hydrolyzed *Populus* sections to non-hydrolyzed controls using quantitative fluorescence analysis in confocal laser scanning microscopy (CLSM) and surface chemical analysis in time-of-flight secondary ion mass spectrometry (TOF-SIMS).

Experimental

Microbial strains and culture media

Clostridium thermocellum (ATCC 27405) was maintained in the laboratory in 20% glycerol stocks at $-80\text{ }^{\circ}\text{C}$. For batch growth, MTC culture media were prepared as previously described.¹⁶

Poplar sectioning, extractive removal and carbohydrate content analysis

Populus deltoides was grown in an ORNL greenhouse at $25\text{ }^{\circ}\text{C}$ with 16 h day light for approximately 180 days before harvesting 10–12 inches of the stem. *Populus* stems ($\sim 4\text{ cm}$ length, $\sim 2\text{ cm}$ diameter) were cross-sectioned to 60 μm thick slices using a LEICA CM 1850 cryostat with an OCT compound (Tissue-TEK) embedding material and an acetone-wiped disposable steel blade. *Populus* sections underwent Soxhlet extraction overnight with dichloromethane to remove the extractives

in the lignocellulosic biomass. The carbohydrate content of raw, control and fermented poplar biomass was determined by quantitative saccharification assay NREL/TP-510-42618 and HPLC method NREL/TP-510-42623, as previously described.¹⁶ In short, biomass solids were acid hydrolyzed by successive treatment in 72% and 4% w/w H_2SO_4 and the resulting soluble sugars were separated and quantified by liquid chromatography against known standards using an AminexTM HPX-87P column (Bio-Rad Laboratories Inc., CA). Sugar degradation products (furfural and 5-hydroxymethyl furfural) were also quantified against known standards to ensure optimal acid solubilization with only trace amounts of degradative products detected.

Microbial bioconversion of poplar and fermentation yields

Microtome-sections of extractive-free poplar were used (at 10 g L^{-1} , dry weight basis) as the carbohydrate source in the anaerobic preparation of MTC media for batch microbial bioconversions (ESI Fig. S1†). To obtain fermented poplar samples, freshly grown *C. thermocellum* was used as the inoculum at 10% v/v and the bottles were incubated at $60\text{ }^{\circ}\text{C}$ for 92 h with gentle shaking (MaxQTM 6000 Incubator Shaker, ThermoFisher Scientific, MA). Fermentations were performed in triplicate biological replication. Control poplar biomass was processed similarly in a single bottle without receiving a microbial inoculum. Replicate processing of control poplar was not needed, as a previous study¹⁶ indicated that short-term storage in buffered medium does not induce significant changes in the solids to warrant investigation of the variation. However, all further analyses of control poplar biomass were performed in technical replication as indicated.

Aliquots of the liquid supernatant of the incubated cultures were collected at $\sim 24\text{ h}$ intervals and the fermentation products and potential solubilized hydrolysis sugars were determined by HPLC against known standards of ethanol, acetic acid, formic acid, lactic acid, cellobiose, glucose and xylose. In short, samples were filtered ($0.22\text{ }\mu\text{m}$), and then acidified to pH 2 with 2 M H_2SO_4 . Separation was made at a 0.5 mL min^{-1} flow rate with a 5 mM H_2SO_4 mobile phase through an Aminex HPX-87H column (Bio-Rad Laboratories Inc., CA) at $60\text{ }^{\circ}\text{C}$ and the products were quantified by the refracting index at $50\text{ }^{\circ}\text{C}$ (detector model L-2490, Hitachi High Technologies America Inc., IL). Soluble sugars were not detectable in the incubated culture medium and only acetic acid and ethanol were produced by fermentation at above threshold concentrations.

Enzymatic hydrolysis with purified cellulase exoproteome

Affinity purified *C. thermocellum* cellulase exoproteome¹² was graciously donated by Yannick J. Bomble (National Renewable Energy Laboratory, CO). Biomass residues of fermented and control poplar were washed four times in sterile buffer (pH = 7.4) made of 50 mM Tris, 100 mM NaCl and 5 mM CaCl_2 , in order to remove microbes and their enzymes from the surface – the absence of attached microbes in washed biomass was later verified by scanning electron microscopy. Enzymatic hydrolysis of the washed control and fermented poplar was

performed in five biological replicates each and involved suspending the biomass in a freshly prepared buffer (pH = 5.5) made of 20 mM sodium acetate, 5 mM CaCl₂, 100 mM NaCl, 2 mM EDTA, and 10 mM L-cysteine-HCl, as previously described.¹² The *C. thermocellum* cellulase exoproteome was then added at 20 mg protein per g biomass, a concentration range similar to a published work,¹¹ where excellent activity was demonstrated on model cellulose and dilute-acid pretreated corn stover. Additionally, a commercial *Aspergillus niger* β-glucosidase (Novozyme 188 with 250 units per g Sigma-Aldrich, MO) was added at 20 μL β-glucosidase solution per g biomass to avoid cellobiose inhibition of cellulases. Enzymatic hydrolysis was performed at 60 °C for 96 h with shaking and the end-point solute sugars were quantified by HPLC as previously detailed. To account for the potential presence of oligomeric sugar hydrolysates, aliquots of the hydrolysis supernatant were also acid-hydrolyzed with 4% H₂SO₄ for 1 h at 120 °C and then neutralized to pH ~ 2.1 with 50% w/w NaOH. The resulting monosaccharides were quantified by HPLC as described. No significant increase in total glucose was detected with this extra acid-hydrolysis of solutes; however, additional xylose was detected from supernatant xylooligomers and was reported accordingly.

Confocal laser scanning microscopy for quantitative fluorescence and colocalization analyses

Control and fermented poplar samples were washed and rinsed three times in sterile saline solution. To fluorescently label the cellulose, six controls and six fermented poplar cross-sections (randomly selected from biological replicate bottles) were then placed in saline solutions with 18 μM Direct Red 23 (Sigma-Aldrich, MO) and allowed to stain for 10 minutes in the dark. The dye solution was then replaced twice with a fresh saline liquid to rinse the excess DR23 from biomass. Poplar sections were then blot-dried gently and mounted with antifade oil (SlowFade Diamond Antifade Mountant, Life Technologies, CA) onto microscope slides with coverslips. Confocal laser scanning microscopy (Zeiss LSM 710, Carl Zeiss AG, Germany) was used to acquire at least two z-stack volume scans at random positions in each poplar section.

To adhere to strict quantitative imaging principles, all samples were scanned with identical instrument settings using: Plan-Apochromat 63×/1.40 NA oil immersion objective, laser excitation at 405 nm wavelength and 45% power and 488 nm wavelength with 15% power; pinhole size of 1 AU (airy units), detector bandpass filters of 410–480 nm to capture lignin autofluorescence and 550–625 nm to capture DR23 fluorescence with the corresponding beam-splitters and detector gains set to 863 and 660, respectively. Volume z-stack scans – ranging between 10 to 14 μm depth – were acquired by capturing images with 0.132 μm per pixel scaling at 0.600 μm z-step size (*i.e.*, at an estimated 50% sectioning overlap between consecutive scans) and a 1.58 μs pixel dwell time. Digital gain and offset were set to default 1 and 0, respectively. These settings were pre-optimized (using real-time pixel intensity histograms) to capture sample emission with minimal pixel saturation

(detector saturation, on an 8-bit scale) and to reduce noise, scan averaging of 2 in line mode was performed.

Volume 3D views were reconstructed in Zen Black 2.1 (Carl Zeiss AG, Germany) in transparency rendering mode using a signal threshold of 5, ramp 9, maximum opacity of 80% and brightness 2.1.

For quantitative fluorescence and colocalization imaging, signal data were used raw, as acquired and extracted using ImageJ in the Fiji distribution package.¹⁹ First, a z-stack of 3 μm (5 frames of 0.600 μm each) was extracted from each independent volume scan to compare regions of identical size (*i.e.*, *x*:*y*:*z* of 134.82 μm : 134.82 μm : 3.00 μm). To eliminate user bias, the extracted z-stack was always centered on the frame with the highest average pixel intensity for cellulose (*i.e.*, the middle slice in the 5-slice stack had the most intense fluorescence emission in the original z-stack). The signal was captured and analyzed in an 8-bit scale (*i.e.*, a range of 0–255 pixel intensity distribution).

Pearson's *r* coefficient and Manders' split coefficient

ImageJ plugin “coloc 2” (part of the Fiji distribution package) was used to calculate the Pearson's *r*²⁰ and Manders'²¹ coefficients according to the user guidelines (http://imagej.net/Coloc_2). Each image analyzed was composed of 5-frame z-stacks. Pixel thresholds were auto-detected and all Pearson's correlations were validated according to Costes theory and significance tests.²⁰

Colocalization across the plant cell wall

In volume scans made of 5 z-stack frames, a region of interest of variable length in μm and of exactly 2.5 μm widths was drawn across three adjacent plant cells such that the length axis was intersecting the cell wall at a perpendicular axis (ESI Fig. S2†). Pixel intensity was averaged in the width dimension and between the 5 frames of a z-stack and plotted against the length axis.

Spatially-resolved average fluorescence intensity

To reduce background noise from non-tissue areas, minimum thresholds were set to 17 and 26 for cellulose-DR23 and lignin signals, respectively. The average signal fluorescence intensity was calculated as:

$$\sum_{i=1}^5 \frac{\sum_{j=\text{threshold}}^{255} (pxI_j \cdot pxC_j)}{\sum_{j=\text{threshold}}^{255} pxC_j}$$

where *i* is the frame number (for a total of 5 frames in a z-stack), *j* is the intensity scale in 8-bit, *pxI* is the pixel intensity and *pxC* is the pixel count. Calculations were made separately for each detection channel and the results of six randomly selected z-stacks were averaged.

Average localization distance across cell walls (from lumen to lumen)

For each detection channel, the distance across the cell walls captured in the regions of interest shown by the histograms was measured as the difference in μm between the start and the end of cellulose or lignin signals with a minimum average intensity of 5.

Surface analysis by chemical spectroscopy

A Bi_3^{2+} primary ion beam from a TOF-SIMS V (ION-TOF, Münster, Germany) instrument was randomly rastered across the *Populus* cross-sections and the ejected secondary ions were analyzed in positive mode to produce a spectrum or an image. A total of 7 different $500 \times 500 \mu\text{m}$ area (128×128 pixels) locations on 2 control and 2 fermented cross-sections were analyzed in bunch mode to determine the normalized ion intensities. The ToF-SIMS images were similarly obtained, but using the burst alignment mode at 256×256 pixels and $100 \times 100 \mu\text{m}$ areas. The normalized ion intensities utilized the average cellulose (m/z 127 and 145), syringyl (S) lignin (m/z 167 and 181), and guaiacyl (G) lignin (m/z 137 and 151) fragmentation ion peaks from 7 different locations, while the ToF-SIMS images converted the ion intensities from these specific fragmentations into a spatial map using a color scale illustrated low (black) to high (yellow/white) intensity. The fraction of normalized ion counts takes into account 24 additional ion peaks associated with polysaccharides and lignin.^{22,23} The average sums of the polysaccharide (PS) and lignin (L) ion peaks are used to calculate the sugar ($\text{PS}/(\text{PS} + \text{L})$) and lignin ($\text{L}/(\text{L} + \text{PS})$) normalized ion count fraction. It is important to note that previously reported xylan ion peaks²⁴ did not in fact characterize hemicellulose. The total polysaccharide fraction reported in this study, which included cellulose and holocellulose, utilized all polysaccharide peaks identified in recent literature.²²

Results

Juvenile *Populus deltoides* stems were sectioned in uniform slices of $60 \mu\text{m}$ thickness (**raw poplar**). Extractive-free poplar was incubated at $60 \text{ }^\circ\text{C}$ for 92 h with microbe-free sterile media (**control poplar**) and with biomass-fermenting *Clostridium thermocellum* 27405 cells (**fermented poplar**) and the residual biomass of these two treatments was analyzed for content and structure.

The carbohydrate content of non-extracted raw tissue was typical of poplar composition (Table 1) with glucan accounting for the bulk sugar biopolymer. Biomass extractives and ash – as non-structural elements – make up less than 5% of the dry weight content;¹ their removal produced a small increase in the relative proportion of carbohydrates in control biomass. As expected and predicted by the intrinsic recalcitrant nature of lignocellulose, microbial hydrolysis and fermentation of extractive-free and otherwise non-pretreated poplar produced only a modest ($p < 0.05$) reduction in the relative glucan content of the residual fermented tissue (Table 1). This indicated that the residual poplar tissue still retained most of its bulk chemical composition.

Compared to control poplar, microbial hydrolysis solubilized 17% (w/w) of the total solids (on a dry weight basis), the majority (83%) of which was glucan. The predominant removal of glucan owed in part to the preservation of the plant cell wall structure during cryotome sectioning, which exposed polysaccharide-rich regions in the S2 and S3 layers (lumen side) of secondary cell walls (Fig. 1).^{25,26}

Overall, the limited hydrolysis removed 22% of the total sugar equivalents supplied in the lignocellulosic material, with predominant consumption of six-carbon sugars (glucose, galactose, and mannose) and to a lesser degree of five-carbon sugars (Table 2). We note that glucan and mannan recorded the similar percent reduction, which may be related to the closer association between these polysaccharides in the secondary cell wall.

Microbial utilization of solubilized glucan yielded detectable fermentation products in typical amounts and ratios (Fig. 2) with ethanol calculated at 38% of the maximum theoretical yield (on a soluble glucan basis) – a typical value for wild-type strains under optimal growth conditions.²⁷ Soluble sugars were not detected and did not accumulate in the fermentation supernatant between the slowdown in the fermentation output (48 h) and the end-point measurement (92 h), indicating non-inhibited microbial metabolism, which was not decoupled from hydrolysis. The bio-conversion slowdown was therefore due to a hydrolytic bottleneck.

Control and fermented poplar tissues were washed and exposed to Direct Red 23 (DR23, formerly Pontamine Fast Scarlet 4B), a dye with high selectivity for β -1,4 linked polysaccharides and highly fluorescent upon cellulose binding, while significantly less fluorescent when bound to xyloglucan.^{28,29} In

Table 1 Relative polysaccharide content in sectioned poplar biomass

| | Glucan | Xylan | Galactan | Arabinan | Mannan |
|----------------------|------------------|------------------|-------------------|--------------------|-------------------|
| Raw poplar (%) | 43 (± 1.4) | 13 (± 0.8) | 2.4 (± 0.1) | 0.71 (± 0.0) | 1.7 (± 0.0) |
| Control poplar (%) | 45 (± 0.9) | 14 (± 0.4) | 2.3 (± 0.2) | 0.60 (± 0.1) | 1.9 (± 0.0) |
| Fermented poplar (%) | 40 (± 1.1) | 16 (± 0.4) | 2.3 (± 0.2) | 0.70 (± 0.1) | 1.5 (± 0.1) |

Sugars in %, g g^{-1} biomass (\pm standard deviation) in the initial unprocessed biomass (raw poplar) and in the extractive-free biomass incubated in buffered growth-medium without microbes (control poplar) and with *Clostridium thermocellum* (fermented poplar) for 92 h at $60 \text{ }^\circ\text{C}$. Fermentations and quantitative analysis of the sugar content performed in triplicate biological replication.

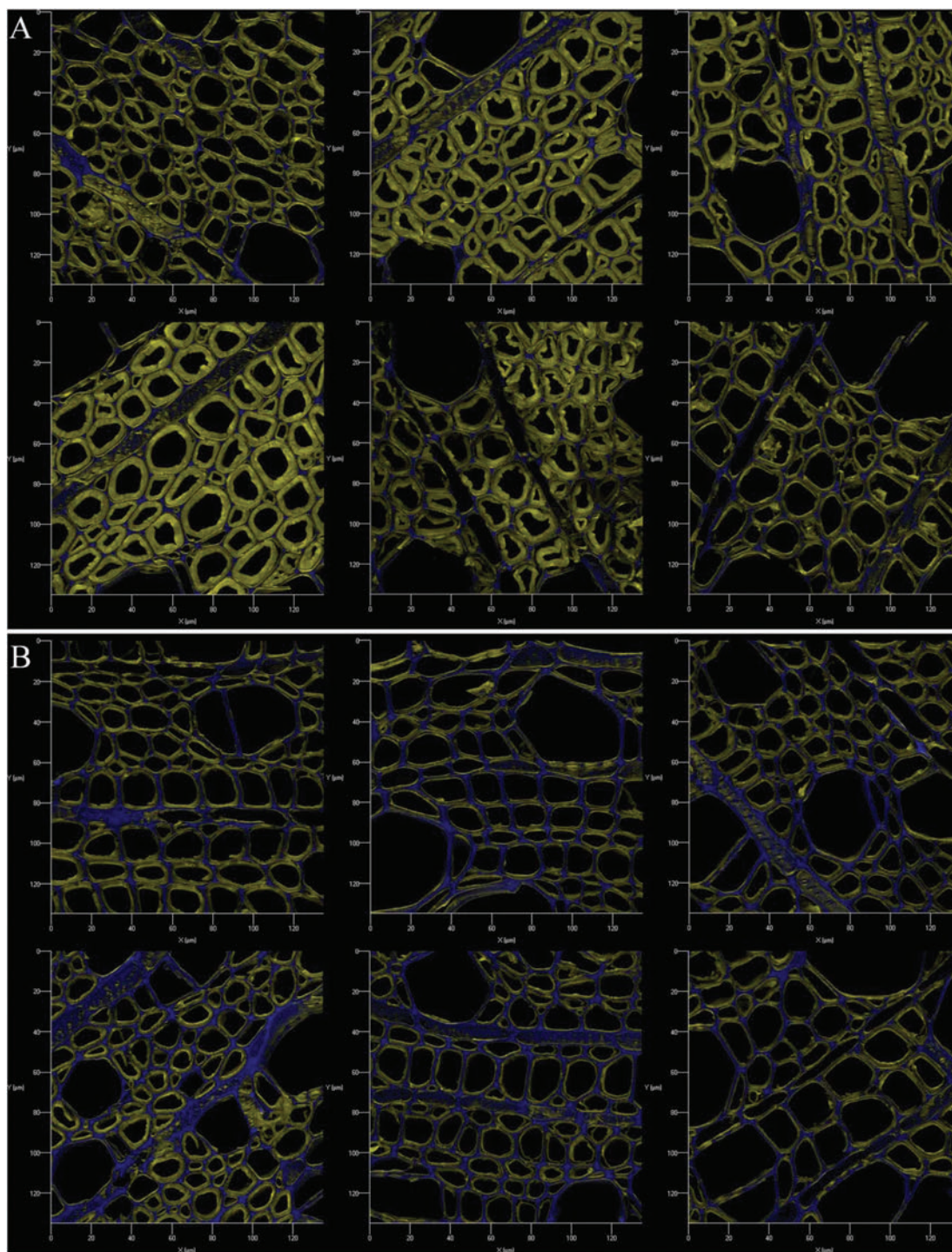


Fig. 1 Confocal laser scanning micrographs of the control (A) and fermented biomass (B) of cross-sectioned *Populus deltoides* showed the post-fermentation reduction of cellulose signals (yellow) in secondary cell walls, which revealed undigested lignin (blue). Cellulose labeled with Direct Red 23 (formerly, Pontamine Fast Scarlet 4B), lignin was autofluorescent.

confocal laser scanning microscopy, DR23 emission was captured in the 550–625 nm visible spectral band under $\lambda_{\text{exc}} = 488$ nm excitation. Lignin in plant tissue samples was visualized by autofluorescence under $\lambda_{\text{exc}} = 405$ nm excitation in the 410–480 nm emission band. In the experimental conditions

selected, lignin and cellulose-bound DR23 fluorescent signals were independent and not cross-interfering. This was confirmed in spectral scans by the absence of a cross-channel talk between the two, *i.e.*, at $\lambda_{\text{exc}} = 405$ nm lignin had no significant emission above 550 nm, and at $\lambda_{\text{exc}} = 488$ nm no lignin auto-

Table 2 Microbial solubilization of polysaccharides in extractive-free *Populus* after incubation for 92 h at 60 °C

| | Total glucose | Total xylose | Total galactose | Total arabinose | Total mannose | Total six carbon | Total five carbon | Total sugars |
|------------------------|---------------|--------------|-----------------|-----------------|---------------|------------------|-------------------|--------------|
| Control biomass (mg) | 153 | 48 | 7.6 | 2.2 | 6.3 | 167 | 51 | 217 |
| Fermented biomass (mg) | 110 | 47 | 6.3 | 2.0 | 4.3 | 121 | 49 | 170 |
| Percent reduction (%) | 28% | 2.4% | 18% | 7.5% | 33% | 28% | 2.7% | 22% |

Total sugars (mg, monomeric equivalent) in biomass incubated with *Clostridium thermocellum* (fermented biomass) compared to biomass incubated in sterile culture media (control biomass).

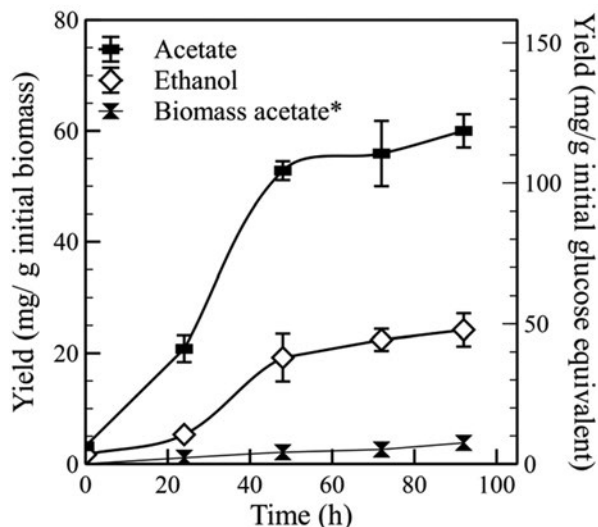


Fig. 2 Fermentation product yields. Microbial fermentation of extractive-free *Populus* incubated with *C. thermocellum* for 92 h at 60 °C yielded ethanol and acetate at a ratio typical of the bacterium wild-type phenotype. Small amounts of biomass-derived acetate were measured for control poplar sections incubated with sterile medium. Biological replication $n = 3$; error bars represent one standard deviation.

fluorescence was detected which is supported by the existing literature.^{30,31}

In the cross-sections, control poplar displayed glucan-rich (yellow) secondary cell walls with lignin-rich (blue) middle lamella between and at the corner of the adjacent cells (Fig. 1A). In several of the examples provided, cellulose-rich

G-layer formations may be observed, a common feature of poplar under normal growth conditions.²⁵ Fermented poplar showed a visually discernible reduction in the cellulose signal near the lumen and a compensatory increase in lignin visibility across cell walls (Fig. 1B). This was confirmed in quantitative fluorescence and colocalization analysis by a significant ($p < 0.05$) increase in the pixel intensity spatial correlation, *i.e.*, the Pearson's r coefficient,²⁰ between lignin and cellulose-DR23 signals in the fermented poplar samples (Table 3).

The Manders' split coefficients,²¹ representative of the fraction of the cellulose-DR23 signal that had an overlapping lignin signal, significantly increased ($p < 0.05$) in fermented poplar to near maximum values with an average 0.92 fractional overlap (Table 3). To better visualize the lignin colocalization with cellulose through secondary cell walls and in particular at the lumen surface, fluorescence intensities were also mapped across cell walls (Fig. 3) at 18 randomly selected positions (ESI Fig. S2†). The localization axis of each box (x -axis, in Fig. 3) cut across three adjacent plant cells, and intersected cell walls (from lumen to lumen, *e.g.*, arrows) and middle lamellas at a perpendicular angle. In control poplar, a strong lignin signal of the middle lamella was flanked on each side by strong cellulose-DR23 fluorescence towards the lumen. Lignin was colocalized with cellulose at low intensity. In fermented samples, lignin strongly colocalized with the cellulose signal throughout the secondary cell walls up to the lumen side, indicative of an increased exposure of the lignin polymer and a decline in surface cellulose.

Quantitative fluorescence of spatially-resolved signals (*i.e.*, averaged pixel intensities normalized to the total counts of pixels with a minimum threshold value, on an 8-bit scale) for

Table 3 Colocalization coefficients of lignin and cellulose in the control and fermented poplar

| Control poplar | Pearson's correlation, r | Manders' split coefficient | Fermented poplar | Pearson's correlation, r | Manders' split coefficient |
|----------------|----------------------------|----------------------------|------------------|----------------------------|----------------------------|
| 1 | 0.28 | 0.80 | 1 | 0.27 | 0.84 |
| 2 | 0.07 | 0.55 | 2 | 0.51 | 0.94 |
| 3 | 0.24 | 0.76 | 3 | 0.50 | 0.95 |
| 4 | 0.00 | 0.47 | 4 | 0.54 | 0.96 |
| 5 | 0.14 | 0.57 | 5 | 0.56 | 0.96 |
| 6 | 0.36 | 0.85 | 6 | 0.39 | 0.87 |
| Avg. | 0.18 | 0.67 | Avg. | 0.46 | 0.92 |

Pearson's r coefficient represents the intensity correlation of colocalizing pixels; Manders' split coefficient represents the fraction of the cellulose-DR23 signal that had an overlapped lignin signal. Measurements made in z -stacks (of five frames) from the images of the randomly sampled poplar are presented in Fig. 1.

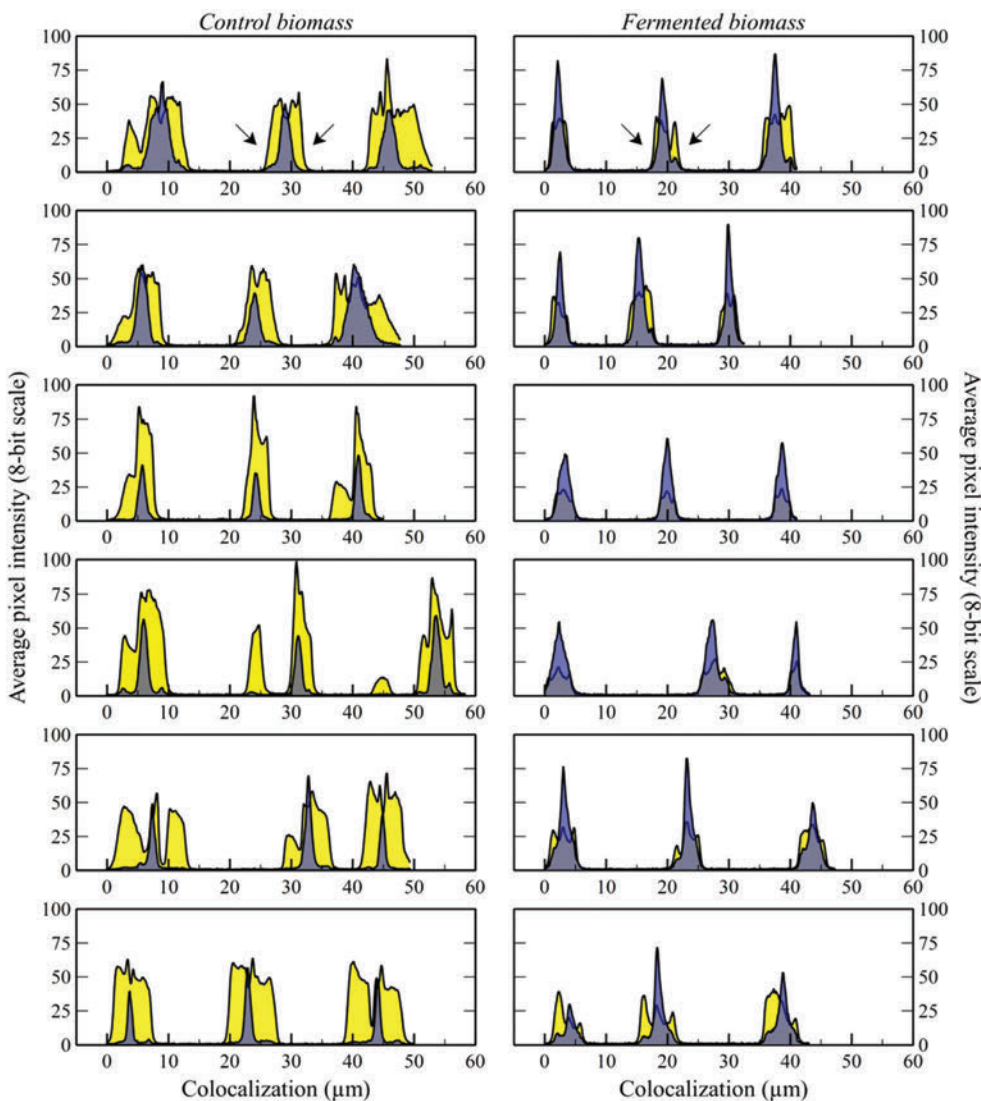


Fig. 3 Colocalization of cellulose and lignin in plant cell walls of the control (left) and fermented biomass (right). Colocalization measured across the walls of adjacent plant cells (from lumen to lumen – e.g., arrows) and each histogram box captures the transverse sectioning of three cell wall regions. Control samples showed cellulose-rich regions on the lumen side (i.e., at the secondary cell wall surface) and strong lignin signal intensity in the central region between the adjacent cells (i.e., in the middle lamella). Post-fermentation, cellulose and lignin signals were well colocalized with high intensity on the lumen side (i.e., at the cell wall surface).

each detection channel (in $n = 6$ randomly captured CLSM scans for each treatment), showed little change in DR23 fluorescence ($p = 0.07$) and an estimated 23% increase ($p < 0.05$) in lignin autofluorescence (Fig. 4). This indicated that cellulose was similarly accessible after microbial hydrolysis to DR23 binding, within the statistical error, which was in line with previous reports that document relatively unchanged chemical bond compositions in carbohydrates following enzymatic hydrolyses.³² The increased signal visibility for the intrinsically autofluorescent lignin was attributed to the removal of surface carbohydrates which obstructed lignin emission, and therefore denotes a higher exposure of superficial lignin.

Cell wall thickness (from lumen to lumen) was highly variable in each treatment (Fig. 4); however, within the $n = 18$

randomly selected measurements, secondary cell wall thinning due to cellulose removal was found within the statistical significance ($p < 0.05$). Variation in the lignin signal location across the cell wall was minimal.

Chemical imaging by ToF-SIMS quantifies and maps the distribution of surface chemical species,²³ which are detected and represented by their ion signatures. This was exemplified as the heat maps of representative ions normalized to the total ion counts (Fig. 5), where under visual inspection, cellulose detection decreased while S- and G-lignin increased post-fermentation. Comparing fermented and control poplar tissue in a more quantitative approach, of $n = 7$ randomly selected regions of poplar cross-sections, revealed an average 49% reduction of cellulose normalized ion counts, and 30% and

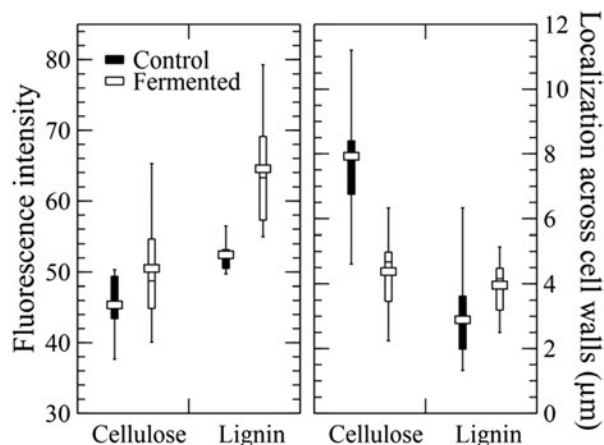


Fig. 4 Average fluorescence intensity of spatially-resolved cellulose and lignin signals (left), as exemplified in Fig. 1, showed the increased visibility of lignin autofluorescence in post-fermentation samples due to surface cellulose removal (left); and estimated localization of cellulose and lignin across the plant cell walls from lumen to lumen (as shown in Fig. 3) confirmed a significant thinning in the presence of cellulose and the persistence of un-digestible lignin. Box plots of measurements in $n = 6$ (left) and $n = 18$ (right) independent and randomly selected samples, whiskers represent the minimum and maximum, vertical solid bars are the interquartile range and the horizontal markers are the means.

11% increase in S- and G-lignin normalized counts, respectively, in the cell walls of microbially hydrolyzed samples (Fig. 6). An extended analysis of 30 ion signatures of polysaccharides and lignin chemical species revealed the inversion of the relative proportions of the two groups, post-fermentation (Fig. 6).

Although initial observations of biomass solubilization (Table 2) and microbial fermentation yields (Fig. 2) indicated a productive microbial metabolism and an otherwise normal growth pattern, the possibility of a solubilization bottleneck due to a stalled cellular metabolism or an enzymatic inhibition was tested. To this end, fermented and control biomass was recovered and cleaned of cells and cellulases by gentle repeated washing with sterile saline solution. The washed biomass was then incubated for four days at 60 °C with the purified (cell-free) cellulase exoproteome of *C. thermocellum* at 20 mg protein per g biomass and commercial *Aspergillus niger* β -glucosidase to test whether hydrolysis resumes equally unobstructed in both the previously fermented and the control feedstock. Results showed that further hydrolysis of the microbially-processed biomass was significantly limited (Fig. 7) confirming an enzymatic bottleneck due to changes in biomass properties demonstrated above.

Discussion

During growth on crystalline cellulose, *C. thermocellum* performs near-complete (95%) solubilization of typical 5 g L⁻¹ Avicel loadings,¹³ and similarly achieved 93% solubilization of industrially-relevant concentrations of 100 g L⁻¹ Avicel.¹⁴

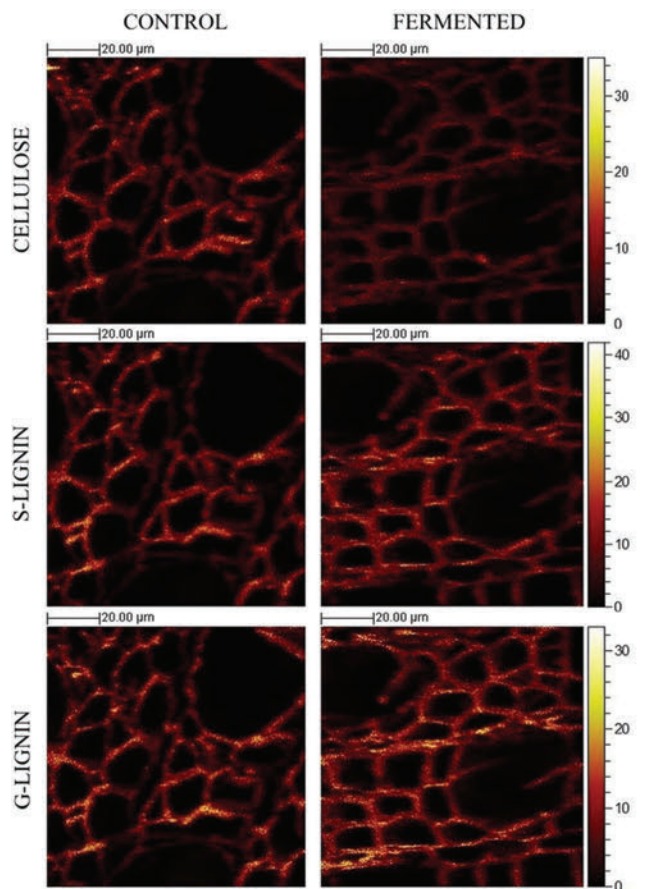


Fig. 5 Sample micrographs obtained by Time-of-Flight Secondary Ion Mass Spectrometry (ToF-SIMS) of the control (left) and fermented (right) biomass of *Populus* cross-sections showed the post-fermentation reduction in surface cellulose and the compensatory increase in S- and G-lignins. The ToF-SIMS technique quantifies and maps the presence of chemical species at the sample surface.

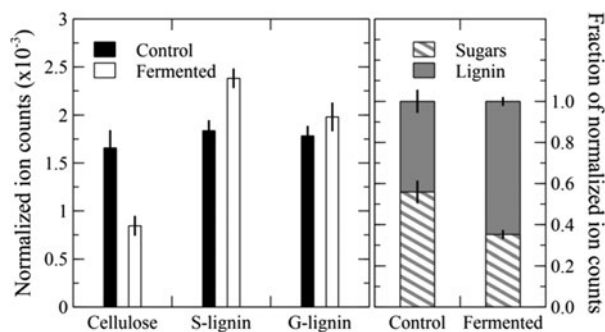


Fig. 6 ToF-SIMS analysis of chemical species at the sample surface revealed a marked decrease in surface cellulose and a compensatory increase in surface S- and G-lignins at the end-point of microbial conversion (left); sum of 30 ion count signatures of known polysaccharide and lignin chemical species represented as the normalized fraction showed the inversion of their relative proportion post-fermentation (right). Data averaged across $n = 7$ randomly selected samples. Ion counts of each chemical species were normalized against the total sample ion counts.

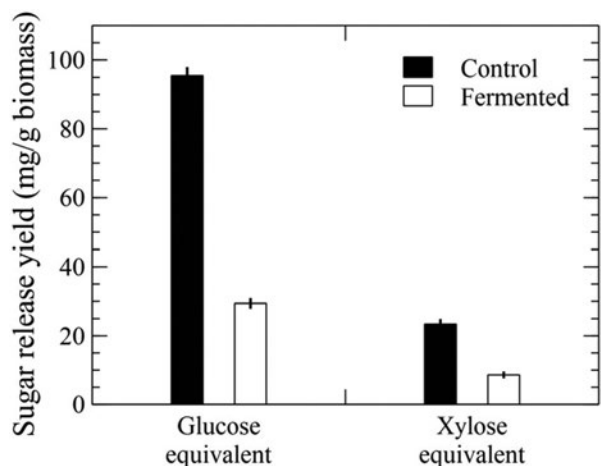


Fig. 7 Sugar release from further hydrolysis of the control and fermented *Populus* biomass with purified, cell-free extracts of *C. thermocellum* cellulases. The *a priori* microbially-fermented biomass with reduced surface cellulose and higher surface lignin yielded significantly lower sugars from further enzymatic hydrolysis compared to control biomass that was not “depleted” by microbes. Biological replication $n = 5$; error bars represent one standard deviation.

However, due in part to its inability to deconstruct lignin in biomass it performs only partial hydrolysis of raw lignocellulosic feedstock. It reached a reported 20% total solids solubilization of non-pretreated poplar¹⁶ – with an estimated 35% glucan and 25% xylan hydrolysis. During growth on non-pretreated senescent switchgrass it attained an estimated 60% solubilization of its glucan and xylan content.¹⁵ Partial hydrolytic activity of raw lignocellulose is common among cellulolytic microbes investigated for biorefinery applications, and microbial hydrolysis compares favorably with the performance of purified commercial fungal enzymes, as exemplified in these reports.

Although the basis for limited hydrolysis is not fully elucidated, and while the causality may be situational, distinct general justifications have been demonstrated. Firstly, cellulases are inhibited by sugar hydrolysates^{4,33} and potentially by lignin-derived phenolic acids (*e.g.* gallic, vanillic, *etc.*).³⁴ Contraction of the hydrolytic activity may also be linked to the inhibition of microbial metabolism by biomass degradation products – carboxylic acids, heterocyclic aldehydes and phenolic derivatives.³⁵ *C. thermocellum* can solubilize xylan to pentoses, which have recently been shown to accumulate intracellularly and inhibit growth and end-product formation in defined media³⁶ and to accumulate intracellularly in switchgrass fermentations.³⁷ Lignin in biomass provides sites for non-specific and non-productive binding of glycoside hydrolases which restricts access to the cell wall sugars and leads to a loss of activity.³⁸ Lastly, cellulases encounter a physical, mechanical barrier to carbohydrate accessibility. In this quantitative study, we separate microbial inhibition from enzymatic inhibition through our use of controls and sequential treatments. We demonstrate that decreases in available surface cellulose

post-fermentation are associated with concomitant increases in surface lignin and enzymatic inhibition of hydrolysis of non-pretreated poplar *via* quantitative analysis CLSM fluorescence images and ToF-SIMS. We hypothesize that if antibodies specific to C5 components (*e.g.* xylan) had been available then similar post-fermentation profiles would have been generated for hemicellulose as compared to cellulose. Consistent with our study, improved hydrolysis of common reed was observed following pretreatments that removed surface lignin as characterized by X-ray spectroscopy (XPS) and ToF-SIMS analyses³⁹ and other studies that significantly reduce the total lignin content and increase biomass porosity.⁴⁰ Additionally, the hydrolytic activity was improved by the mechanical milling of non-pretreated biomass between successive fermentations.¹⁵ In general, a lower content of total bulk lignin in poplar and a higher syringyl to guaiacyl lignin ratio is associated with improved enzymatic solubilization.^{8,16}

The former limitation imposed by soluble inhibitory compounds can be relieved by mitigating their accumulation and by the metabolic engineering and the directed evolution of resistant microbial strains. In a previous study,¹⁶ metabolic inhibitors towards *C. thermocellum* were not detected when grown on non-pretreated *Populus* at similar or higher loadings to the current analysis and our fermentative performance further indicated unrestricted metabolism. Similarly, cellulase inhibition by soluble components was invalidated by the results of Fig. 7, where the hydrolytic activity on washed residual biomass could not be significantly restored with cell-free cellulase preparations although the biomass still retained 72% of the original glucan content when compared to the control sample.

The latter two constraints to hydrolysis are intrinsic to the properties of ordinary biomass, namely the synthesis of lignin in the plant cell wall structure. On the principle that an increased lignin content in bulk tissue of milled poplar strongly correlates with reduced enzymatic solubilization,⁸ we further provide direct, quantitative evidence that microbial hydrolysis was suspended by a higher exposure of the lignin to the feedstock surface after the initial limited removal of accessible carbohydrates. Fluorescent labelling of *Trichoderma reesei* Cel7A has indicated preferential binding of the enzyme to the delignified regions of lignocellulosic feedstock.⁴¹ Conversely, glycoside hydrolases are known to non-specifically bind lignin. In a recent report,³⁸ β -D-glucosidases and xylanases, which do not contain carbohydrate-binding modules, showed the highest binding affinity to lignin; however, this non-specific binding only resulted in a very modest (4–15%) decrease in the activity of these enzymes. We attempted cellulase adsorption measurements by BCA assay on fermented and control biomass without success due to interferences from matrix components (*e.g.*, reduced sugars). Although we cannot comment whether enzyme binding was affected by higher lignin exposure we have demonstrated nonetheless that cellulases were significantly less productive.

It is interesting to note that strong limitation to hydrolysis occurred when the surface cellulose decreased to approxi-

mately half of its initial value. In ToF-SIMS analysis, total ion signatures of surface lignin species (Fig. 6) showed an increase in relative proportion from 44% in control to 65% in fermented tissue. These are surprising novel observations of feedstock surface chemistry, which point to the severity of lignin interfering with sugar accessibility. Feedstock improvement strategies that reduce the bulk lignin content can only partially relieve these accessibility constraints, as seen in the down-regulation of a lignin biosynthetic gene,⁴² which led to a *ca.* 20% improved hydrolysis.⁴³ While stringent chemical pre-treatment conditions have been effective, we strongly recommend that bio-based conversion technologies combine carbohydrate solubilization strategies with novel methods of concurrent or step-wise depolymerization of surface-exposed lignin.

Conclusion

In conclusion, we assert that microbial hydrolysis of raw woody feedstock is arrested prematurely by a critical shift in the ratio of carbohydrates and lignin at the biomass surface whereby the internal regions of the plant tissue may retain a relatively unaltered chemical composition. Although these “depleted surfaces” lead to non-productive enzymes, it remains to be seen to what extent it impacts specific and non-specific cellulase binding. The direct evidence produced in the study provides an explicit definition of the concept of feedstock recalcitrance and represents a new platform to study plant tissue properties that impact biological solubilization.

Acknowledgements

We thank Yannick J. Bomble (National Renewable Energy Laboratory) for the donation of *C. thermocellum* purified cellulases. We thank Udaya C. Kalluri (ORNL) for providing the juvenile poplar. This research was funded by the Bioenergy Science Center (BESC) which is a U.S. Department of Energy Bioenergy Research Center supported by the Office of Biological and Environmental Research in the DOE Office of Science. ORNL is managed by UT-Battelle, LLC, Oak Ridge, TN, USA, for the DOE under contract DE-AC05-00OR22725. A. T. is grateful for the financial support from the Paper Science & Engineering (PSE) fellowship program at the Renewable Bioproducts Institute at the Georgia Institute of Technology. This manuscript has been authored by UT-Battelle, LLC under contract no. DE-AC05-00OR22725 with the U.S. Department of Energy. The United States Government retains and the publisher, by accepting the article for publication, acknowledges that the United States Government retains a non-exclusive, paid-up, irrevocable, world-wide license to publish or reproduce the published form of this manuscript, or allow others to do so, for United States Government purposes. The Department of Energy will provide public access to these results of federally sponsored research in accordance with

the DOE Public Access Plan (<http://energy.gov/downloads/doe-public-access-plan>).

Notes and references

- 1 P. Sannigrahi, A. J. Ragauskas and G. A. Tuskan, *Biofuels, Bioprod. Biorefin.*, 2010, **4**, 209–226.
- 2 B. Erickson, J. E. Nelson and P. Winters, *Biotechnol. J.*, 2012, **7**, 176–185.
- 3 U. S. Department of Energy, M. H. Langholtz, B. J. Stokes and L. M. Eaton, 2016 Billion-Ton Report: Advancing Domestic Resources for a Thriving Bioeconomy, Volume 1: Economic Availability of Feedstocks, Oak Ridge, TN, 2016, vol. 1.
- 4 J. S. Van Dyk and B. I. Pletschke, *Biotechnol. Adv.*, 2012, **30**, 1458–1480.
- 5 V. Mbaneme-Smith and M. S. Chinn, *Energy Emiss. Control Technol.*, 2015, 23–44.
- 6 A. J. Ragauskas, G. T. Beckham, M. J. Bidy, R. Chandra, F. Chen, M. F. Davis, B. H. Davison, R. a. Dixon, P. Gilna, M. Keller, P. Langan, A. K. Naskar, J. N. Saddler, T. J. Tschaplinski, G. a. Tuskan and C. E. Wyman, *Science*, 2014, **344**, 1246843–1246843.
- 7 Y. Zeng, S. Zhao, S. Yang and S.-Y. Ding, *Curr. Opin. Biotechnol.*, 2014, **27**, 38–45.
- 8 M. H. Studer, J. D. DeMartini, M. F. Davis, R. W. Sykes, B. Davison, M. Keller, G. A. Tuskan and C. E. Wyman, *Proc. Natl. Acad. Sci. U. S. A.*, 2011, **108**, 6300–6305.
- 9 M. Zhang, X. Ju, X. Song, X. Zhang, Z. J. Pei and D. Wang, *Bioresour. Technol.*, 2015, **194**, 407–410.
- 10 L. R. Lynd, P. J. Weimer, W. H. van Zyl and I. S. Pretorius, *Microbiol. Mol. Biol. Rev.*, 2002, **66**, 506–577.
- 11 E. A. Bayer, R. Lamed, B. A. White and H. J. Flint, *Chem. Rec.*, 2008, **8**, 364–377.
- 12 Q. Xu, M. G. Resch, K. Podkaminer, S. Yang, J. O. Baker, B. S. Donohoe, C. Wilson, D. M. Klingeman, D. G. Olson, S. R. Decker, R. J. Giannone, R. L. Hettich, S. D. Brown, L. R. Lynd, E. A. Bayer, M. E. Himmel and Y. J. Bomble, *Sci. Adv.*, 2016, **2**, e1501254.
- 13 L. D. Ellis, E. K. Holwerda, D. Hogsett, S. Rogers, X. Shao, T. Tschaplinski, P. Thorne and L. R. Lynd, *Bioresour. Technol.*, 2012, **103**, 293–299.
- 14 E. K. Holwerda, P. G. Thorne, D. G. Olson, D. Amador-Noguez, N. L. Engle, T. J. Tschaplinski, J. P. van Dijken and L. R. Lynd, *Biotechnol. Biofuels*, 2014, **7**, 155.
- 15 J. M. D. Paye, A. Guseva, S. K. Hammer, E. Gjersing, M. F. Davis, B. H. Davison, J. Olstad, B. S. Donohoe, T. Y. Nguyen, C. E. Wyman, S. Pattathil, M. G. Hahn and L. R. Lynd, *Biotechnol. Biofuels*, 2016, 1–13.
- 16 A. Dumitrache, H. Akinosho, M. Rodriguez, X. Meng, C. G. Yoo, J. Natzke, N. L. Engle, R. W. Sykes, T. J. Tschaplinski, W. Muchero, A. J. Ragauskas, B. H. Davison and S. D. Brown, *Biotechnol. Biofuels*, 2016, **9**, 31.

- 17 X. Shao, M. Jin, A. Guseva, C. Liu, V. Balan, D. Hogsett, B. E. Dale and L. Lynd, *Bioresour. Technol.*, 2011, **102**, 8040–8045.
- 18 J. K. Saini, A. K. Patel, M. Adsul and R. R. Singhanian, *Renewable Energy*, 2016, **98**, 29–42.
- 19 J. Schindelin, I. Arganda-Carreras, E. Frise, V. Kaynig, M. Longair, T. Pietzsch, S. Preibisch, C. Rueden, S. Saalfeld, B. Schmid, J.-Y. J.-Y. Tinevez, D. J. White, V. Hartenstein, K. Eliceiri, P. Tomancak, A. Cardona, K. Liceiri, P. Tomancak and A. Cordona, *Nat. Methods*, 2012, **9**, 676–682.
- 20 S. V. Costes, D. Daelemans, E. H. Cho, Z. Dobbin, G. Pavlakis and S. Lockett, *Biophys. J.*, 2004, **86**, 3993–4003.
- 21 E. M. M. Manders, F. J. Verbeek and J. A. Aten, *J. Microsc.*, 1993, **169**, 375–382.
- 22 R. E. Goacher, D. Jeremic and E. R. Master, *Anal. Chem.*, 2011, **83**, 804–812.
- 23 R. E. Goacher, E. A. Edwards, A. F. Yakunin, C. A. Mims and E. R. Master, *Anal. Chem.*, 2012, **84**, 4443–4451.
- 24 P. Fardim and N. Durán, *Colloids Surf., A*, 2003, **223**, 263–276.
- 25 M. Schmidt, A. M. Schwartzberg, P. N. Perera, A. Weber-Bargioni, A. Carroll, P. Sarkar, E. Bosneaga, J. J. Urban, J. Song, M. Y. Balakshin, E. A. Capanema, M. Auer, P. D. Adams, V. L. Chiang and P. J. Schuck, *Planta*, 2009, **230**, 589–597.
- 26 L. A. Donaldson and J. P. Knox, *Plant Physiol.*, 2012, **158**, 642–653.
- 27 R. Biswas, T. Zheng, D. G. Olson, L. R. Lynd and A. M. Guss, *Biotechnol. Biofuels*, 2015, **8**, 20.
- 28 C. T. Anderson, A. Carroll, L. Akhmetova and C. Somerville, *Plant Physiol.*, 2010, **152**, 787–796.
- 29 J. Thomas, M. Ingerfeld, H. Nair, S. S. Chauhan and D. A. Collings, *Wood Sci. Technol.*, 2013, **47**, 59–75.
- 30 K. Radotic, A. Kalauzi, D. Djikanovic, M. Jeremic, R. M. Leblanc and Z. G. Cerovic, *J. Photochem. Photobiol. B*, 2006, **83**, 1–10.
- 31 H. Vavrčik, V. Gryc and M. Rybníček, in *Dendro Symposium*, ed. D. Elferts, G. Brumelis, H. Gärtner, G. Helle and G. Schleser, GFZ Potsdam, Scientific Technical Report STR 08/05, Potsdam, 2008, pp. 149–153.
- 32 M. Á. B. Alcántara, J. Dobruchowska, P. Azadi, B. D. García, F. P. Molina-Heredia and F. M. Reyes-Sosa, *Biotechnol. Biofuels*, 2016, **9**, 207.
- 33 Q. Xu, A. Singh and M. E. Himmel, *Curr. Opin. Biotechnol.*, 2009, **20**, 364–371.
- 34 N. Frederick, N. Zhang, X. Ge, J. Xu, M. Pelkki, E. Martin and D. J. Carrier, *ACS Sustainable Chem. Eng.*, 2014, **2**, 1835–1842.
- 35 E. Palmqvist and B. Hahn-Hägerdal, *Bioresour. Technol.*, 2000, **74**, 25–33.
- 36 T. J. Verbeke, R. J. Giannone, D. M. Klingeman, N. L. Engle, T. Rydzak, A. M. Guss, T. J. Tschaplinski, S. D. Brown, R. L. Hettich and J. G. Elkins, *Sci. Rep.*, 2017, **7**, 43355.
- 37 S. Poudel, R. J. Giannone, M. Rodriguez, B. Raman, M. Z. Martin, N. L. Engle, J. R. Mielenz, I. Nookaew, S. D. Brown, T. J. Tschaplinski, D. Ussery and R. L. Hettich, *Biotechnol. Biofuels*, 2017, **10**, 14.
- 38 J. M. Yarbrough, A. Mittal, E. Mansfield, L. E. Taylor, S. E. Hobdey, D. W. Sammond, Y. J. Bomble, M. F. Crowley, S. R. Decker, M. E. Himmel and T. B. Vinzant, *Biotechnol. Biofuels*, 2015, **8**, 214.
- 39 H. Y. Mou, E. Heikkilä and P. Fardim, *Bioresour. Technol.*, 2013, **150**, 36–41.
- 40 G. Brodeur, E. Yau, K. Badal, J. Collier, K. B. Ramachandran and S. Ramakrishnan, *Enzyme Res.*, 2011, 1–17.
- 41 J. S. Luterbacher, J. M. Moran-Mirabal, E. W. Burkholder and L. P. Walker, *Biotechnol. Bioeng.*, 2015, **112**, 32–42.
- 42 C. Fu, J. R. Mielenz, X. Xiao, Y. Ge, C. Y. Hamilton, M. Rodriguez, F. Chen, M. Foston, A. Ragauskas, J. Bouton, R. A. Dixon and Z.-Y. Wang, *Proc. Natl. Acad. Sci. U. S. A.*, 2011, **108**, 3803–3808.
- 43 A. Dumitrache, J. Natzke, M. Rodriguez, K. L. Yee, O. A. Thompson, C. R. Poovaiah, H. Shen, M. Mazarei, H. L. Baxter, C. Fu, Z.-Y. Wang, A. K. Biswal, G. Li, Y. Tang, C. N. Stewart, R. A. Dixon, R. S. Nelson, D. Mohnen, J. Mielenz, S. D. Brown and B. H. Davison, *Plant Biotechnol. J.*, 2016, 1–10.